

Microelectrode Array for the Dielectrophoretic Orientation of C2C12 Myoblast Cells

Douglas Hanson^{a*}, Charles Baker^b, Arturo Ayon^c, Waldemar Gorski^d

^{a,d}*Department of Chemistry, The University of Texas at San Antonio, One UTSA Circle, San Antonio, TX 78249, USA*

^b*Southwest Research Institute, 6220 Culebra Road, San Antonio, TX 78238, USA*

^c*Department of Physics and Astronomy, The University of Texas at San Antonio, One UTSA Circle, San Antonio, TX 78249, USA*

^a*Email: Douglas.P.Hanson@gmail.com*

^b*Email: Charles.Baker@swir.org*

^c*Email: Artuo.Ayon@utsa.edu*

^d*Email: Waldemar.Gorski@utsa.edu*

Abstract

An array of interdigitated microelectrodes was modeled, optimized, and tested for the contactless alignment of living biological cells by negative dielectrophoresis (nDEP). The modeling focused on optimizing the x component, $\frac{dE}{dx}$, of potential gradient to maximize the aligning force at minimal electric field to protect fragile cells. The optimized array was tested with micron-sized, hard polymeric beads and soft C2C12 mouse myoblast cells. The array completely aligned the initially random arrangement of beads after 15 s of applying 450 kHz sinewave electrical signal to the electrodes. Under the same conditions, the array was unable to move C2C12 cells due to their strong adhesion to the surface. However, the array was effective at directing the orientation of confluent C2C12 cells during their differentiation into myotubes for the formation of muscle fibers. The aligned myotubes were alive and capable of growth. The proposed approach has a potential for growing continuously oriented viable tissues under the array of microelectrodes.

Keywords: dielectrophoresis; tissue alignment.

* Corresponding author.

1. Introduction

Dielectrophoresis (DEP) is the application of non-uniform electric fields to create a force capable of moving dielectric particles. When used with alternating current, DEP acts as a positive (pDEP) or negative force (nDEP) moving particles toward the high or the low intensity zones of the electric fields, respectively. Unlike electrophoresis that impacts the movement of charged particles; DEP can move neutral particles in a non-uniform electric field. In a uniform electric field, the forces exerted on a dielectric particle cancel out, resulting in no particle movement [1]. DEP has been shown to be useful in many applications including particle separations [2-11], trapping [12-14], sorting [13, 15-17], and directing [1, 18-20].

One of the attractive features of DEP is its potential for a contactless alignment of cells to grow biological tissues. Such aligned tissues are potentially superior to randomly aligned tissues in both their material properties and functions. Typically, contact guidance has been used to direct the orientation of cells, including fibroblasts, cardiac myocytes, smooth muscle cells, neurons, and bone marrow cells [21-24]. In the process of contact guidance, cells are grown on a substrate containing parallel channels. The drawbacks of such approach include orientation only occurring when cells make contact with channel walls [25, 26] and loss of orientation when the cells exceed the channel height [27-29]. In addition, the walls of the channels present a barrier to forming a continuous layer of tissue. Such issues can be avoided with DEP as the forces generated for alignment and orientation are continuous across the substrate and do not require contact.

In the present work, we model, optimize, and test an interdigitated array of microelectrodes as a tool for the fast and contactless alignment of polystyrene beads and orientation of C2C12 myotubes. In contrast to prior studies with polystyrene beads [30-37], the present optimization focuses on maximizing the potential gradient dE/dx generated by the electrode array. Such optimization is necessary to minimize the potentially negative impact of the electric field on living cells.

2. Materials and Methods

2.1 Modeling

As an extension of the electrostatic dipole force to include a frequency response in the form of the Clausius-Mossotti (CM) factor, the DEP force for a particle in an alternating current field was first described by Herbert Pohl [38]. The time averaged DEP force (F_{DEP}) can be described by

$$F_{DEP} = 2\pi R^2 \epsilon_m f_{CM} \nabla E^2 \quad (1)$$

where R is radius of the particle, ϵ_m the absolute permittivity of the medium, f_{CM} the Clausius-Mossotti factor, and E the strength of the applied electric field.

The CM factor is dependent upon the complex permittivity of both the medium and the particle and captures the AC frequency dependence of the DEP force on both the permittivity and the conductivity. The CM factor can

be broken down into both real and imaginary parts representing the in phase and out of phase portions of the response to the electric field. The real part of the CM factor can be described by [38].

$$f_{CM} = \frac{\epsilon_p^*(\omega) - \epsilon_m^*(\omega)}{\epsilon_p^*(\omega) + 2\epsilon_m^*(\omega)} \quad (2)$$

where the factor ϵ^* is described by eq. 3 and determined by the electrical conductivity of the particle or medium (σ), the imaginary number (i) and the frequency of the electric field (ω)

$$\epsilon^* = \epsilon - \frac{i\sigma}{\omega} \quad (3)$$

The previous modeling of electric fields generated by interdigitated electrode arrays has focused on the total field strength [2, 3, 31, 39]. While the DEP force scales with field strength, there can be no force without a field gradient. Due to the symmetry of our device the z gradient $\frac{dE}{dz}$ is zero. The y gradient $\frac{dE}{dy}$ produces a DEP force that is balanced by the normal force from the substrate and, therefore, does not result in particle motion. The only component of the gradient operator that produces particle motion in the interdigitated array is $\frac{dE}{dx}$. For this reason, the present modeling optimizes the magnitude of the x direction gradient $\frac{dE}{dx}$ with changes in array height, electrode to gap size ratio, and array height relative to electrode size.

The optimization of the DEP was done with the finite element software package QuickField (Tera Analysis Ltd, Denmark) by modeling the field strength and gradients under the array of electrodes. The software allowed drawing a device to scale, assigning physical properties (e.g. permittivity) and boundary conditions (e.g. voltage), and generating an output of the field strength over a two or three dimensional space by solving Poisson's equation for electrostatics. A figure of the design parameters is shown below in Figure 1.

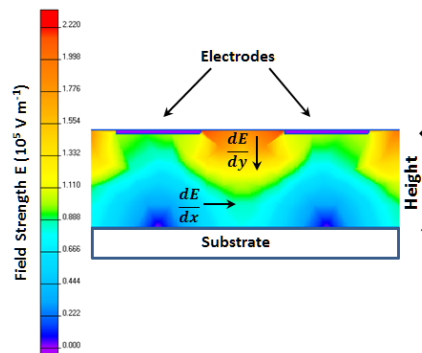


Figure 1: This figure shows the configuration of the modeled device parameters, including the positions of the electrodes, the height of the array above the substrate, and gap between the electrodes.

2.2 Array Fabrication

An interdigitated array of indium tin oxide (ITO) wires was fabricated by photolithography. The glass slides coated with 350-nm thick ITO film were purchased from SPI Supplies (West Chester, PA; SPI#45402). The

ITO slides were spin coated with a positive photoresist (#S1813, Shipley Company; Marlborough, MA) at 900 rpm for 5 s followed by 4000 rpm for 60 s. The photoresist was then baked at 90 °C for 30 min and exposed to a UV source (OAI model 2105C2) with an intensity of 5 mW cm⁻² for 20 s through a photomask containing a the array pattern (CAD/Art Services Inc; Bandon, OR). The array was immersed in a developer solution (MF-24A, Shipley Company; Marlborough, MA) to remove the exposed resist, followed by a bake for 30 min at 120 °C to remove any residual water or developer solution. ITO was removed from the array, to form the gaps by immersion in a mixture of nitric acid, hydrochloric acid, and water in a ratio of 1:5:5 by volume. The remaining resist was then removed from the ITO wires by immersion in a Microposit Remover (1165, Shipley). The ITO array was bonding to a substrate layer, cell culture flask (430372, Corning), using a 100- μ m thick, double sided, copper conductive tape (#16074, 3M). This tape acts as both an electrical conductor to power supply and a spacer to control height between the array and the substrate. Based on the modeling results (sections 3.2 to 3.4), an ITO array with 100- μ m wide electrodes, 100- μ m wide gaps between them, and 100- μ m separation between the electrodes and substrate was used. The 100- μ m separation was enough to allow sufficient space between the cells and the electrode array for the flow of growth media to feed the cells.

2.3 Polystyrene beads

The 5.0 w/v % solution of polystyrene microparticles (6.78 μ m average diameter) with $\epsilon = 2.5$ and $\sigma = 9.4 \times 10^{-5}$ S m⁻¹ was purchased from Spherotech (PP-60-10). Before the analysis, the microparticles were centrifuged at 1300 rpm to separate them from the sodium azide solution and then re-suspended in 18 M Ω ·cm water (at a 1:10 particle-to-water mass ratio).

2.4 C2C12 Mouse myoblast cells

C2C12 Mouse myoblast cells (91031101, Sigma) were grown in growth medium (GM), consisting of Dulbecco's Modified Eagle Medium (D5796, Sigma) supplemented with 10% fetal bovine serum (FBS) (F6178, Sigma), and 1% of penicillin-streptomycin solution (30-2300, ATCC). Differentiation medium (DM) consisted of GM with 2.0 % horse serum (H1270, Sigma) substituted for FBS. All cultures were kept at 37 °C with 5.0 % CO₂. For splitting, cells were collected at 90% confluence by treatment with 20.0 mL of Trypsin/EDTA solution (T4049, Sigma) for 15 minutes. Cells were centrifuged at 600 rpm for 6 minutes and resuspended in GM. Cell count was measured at 7.45 x10⁶ cells per ml with a Hemacytometer (#0267110, Fisher Scientific). Cell viability was determined to be 100% by staining with Typan Blue Solution (SV30084.01, Hyclone).

2.5 Microscopy

A 100- μ L aliquot of solution containing either polystyrene microparticles or C2C12 cells was dispensed into the microfluidic device and allowed to spread under the array. A function generator (BK Precision 4001A) was connected to the copper tape via alligator clips to form a 10 V peak-to-peak AC sine wave with a frequency of 450 kHz. Images were captured either with a LabMed Lx 500 microscope at a 40x magnification (polystyrene) or a Axiovert 135 inverted microscope at a 100x magnification (C2C12 cells), using a 3.0 MP CCD camera (Moticam).

3. Results and Discussion

3.1 Finite Element Modeling

The finite element model was developed to model the DEP forces and optimal geometry of the device. The modeled device consisted of an array of five microelectrodes on the upper surface of a fluid chamber. The modeled area of the device was a two dimensional cross-section (x-y plane) with a fixed width of 1,100 μm (x direction) and a height that ranged from 40 to 200 μm (y direction). The width of electrodes was varied but always remained centered at 150 μm , 350 μm , 550 μm , 750 μm and 950 μm on the x axis. The modeling of electric field strength within the fluid chamber was done by assigning an alternating potential of ± 10 V to the microelectrodes and the relative permittivity of water (80 F m^{-1}) to the fluid chamber. The relevant 3D representation of the 5-electrode array is shown in Figure 2, which illustrates the channels of low field strength along the three inner electrodes marked as 2, 3, and 4.

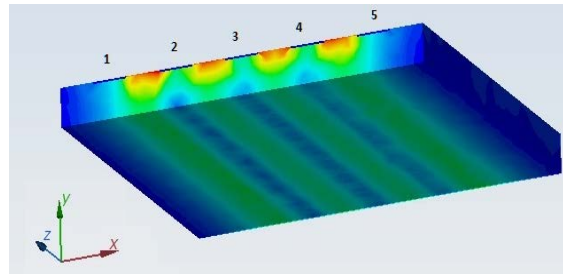


Figure 2: Three-dimensional simulated pattern of electric field strength for a 5-electrode array. Five electrodes are numbered and shown along the top edge as dark blue 100- μm bars.

Figure 3 shows a plot of the simulated electric field strength along the substrate. The values for electric field strength at 1- μm intervals along the substrate in the x direction were used in this simulation. A periodic change in the field strength was observed underneath the electrode array, reaching the maximum value between two adjacent electrodes and a minimum at positions directly below the electrodes. The calculations of the field gradient $\frac{dE}{dx}$ described in the following sections were taken at 500 μm on the x axis, which is the midpoint between the electric field maximum and minimum between the 2nd and 3d electrode. The electric field gradient $\frac{dE}{dx}$ is linear ($R^2 = 0.994$) in a range of ± 40 μm from the midpoint indicating that the DEP force acting on particles in this area should be constant.

3.2 Electrode-to-Gap Ratio Simulations

To determine the effect that changing the electrode-to-gap ratio has on the magnitude of dE/dx , the size of the electrodes and gaps between electrodes was varied in 10 μm increments. The total length of the element (electrode and gap) was fixed at 200 μm . This length allowed generating electrode-to-gap ratios of 0.05 to 3.0 for small electrodes with large gaps or large electrodes with small gaps, respectively. A fixed array height of 100 μm was used in order to allow for particle motion and to be consistent with the thickness of spacer used in the physical device (section 2.2). The results of the simulations are summarized in Figure 4, which shows the

systematic increases in the magnitude of $\frac{dE}{dx}$ in the 0.050-to-1.0 electrode-to-gap range. However, the magnitude of $\frac{dE}{dx}$ leveled out above a 1.0 electrode-to-gap ratio indicating the ratio of 1.0 should provide the maximum benefit.

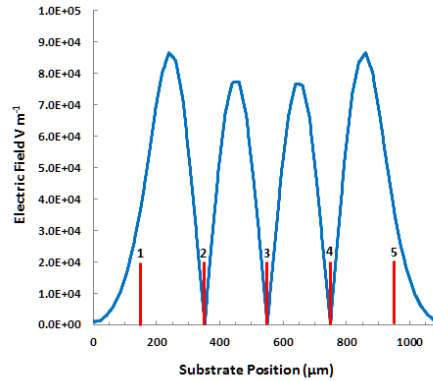


Figure 3: Graph of field strength along the substrate in x direction. The center positions of the five electrodes are shown as red lines to show that the field strength goes to a minimum at positions below the electrodes.

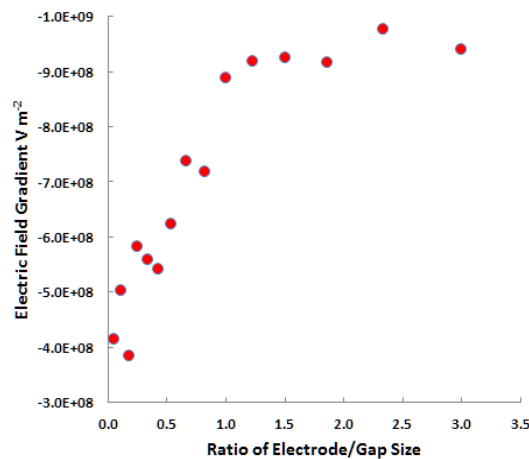


Figure 4: Effect of the electrode-gap ratio on the electric field gradient.

3.3 Electrode Size to Array Height Simulations

The effect of the size of electrodes and gaps on the $\frac{dE}{dx}$ gradient was investigated by using their dimensions in the 25-200 μm range with the electrode-to-gap ratio set at 1.0. The array heights were equal to 75, 100, and 125 μm . The results are summarized in Figure 5, which shows that each simulated array height shows a similar trend of a maximum value near a point where electrode and gap size was equal to the height of the array. In addition, there is a large drop off in field gradient when electrode and gap size are less than half of the array height. This suggested that for any given array height the maximum field gradient was achieved when electrodes, gaps and array height were all of similar size.

3.4 Alignment of 7- μm Polystyrene Particles

In order to demonstrate the merit of the proposed approach, the optimized array device was used to align polystyrene microparticles. The experimental testing of the simulations was performed with a 100- μm high array device having five 100- μm wide electrodes separated by the 100- μm gaps. Before applying DEP, the microparticles that were injected into the array were randomly dispersed (not shown). Upon applying the electrical signal of 450 kHz, a fast movement of the particles was observed. It took only 15 s to reach the alignment shown in Figure 6. In this top down view of the device, looking through the transparent ITO electrodes, it can be seen that the majority of the microparticles (99%) were located perfectly underneath the electrodes of the array indicating that the nDEP force has pushed the particles to low potential regions as predicted by the simulations data in Figures 2 and 3.

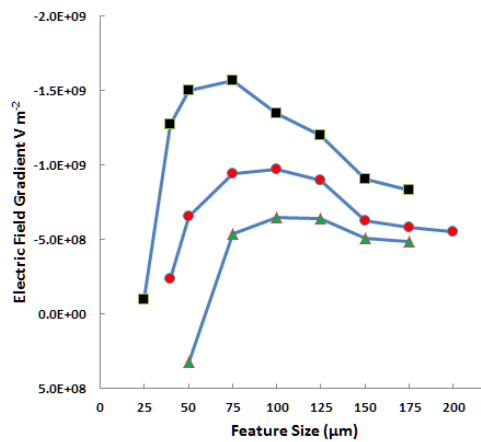


Figure 5: Field gradients of varying electrode and gap size at array heights of 75 (■), 100 (●) and 125 μm (▲). Lines included to guide the eye.

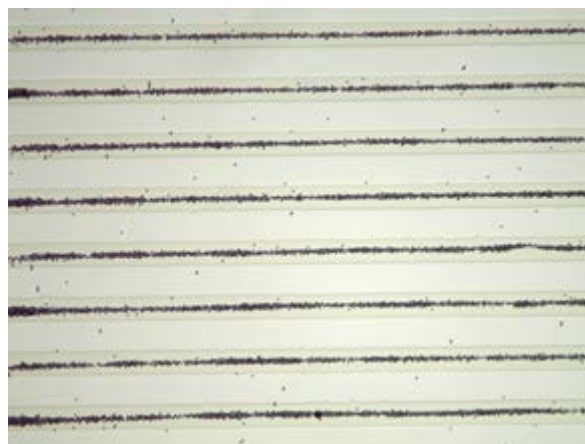


Figure 6: Distribution of 7- μm diameter polystyrene particles after 15 seconds of nDEP at an optimized microelectrode array.

3.5 Alignment and orientation of C2C12 cells

Initial experiments with myoblast cells focused on reproducing the results obtained with polystyrene beads. The hypothesis was that if the cells were first aligned underneath the electrodes, they would subsequently grow and differentiate in an oriented fashion. However, all attempts using a wide range of DEP frequencies (50 kHz-1MHz), surface modifications of substrates, and alterations to the conductivity of the growth medium produced little or no movement of the cells. Apparently, while the y-axis force pushing downward towards the substrate had no effect on a hard polystyrene sphere, it caused the softer biological cells to flatten out and adhere to the substrate preventing their movement. Therefore, another approach was explored. The cells were first allowed to grow to confluence and only exposed to DEP forces during the differentiation phase. Since cells were already in their positions, no translational motion was necessary. During differentiation, the cells were exposed to a DEP field at 450 kHz intermittently for 2 seconds every minute for 12 hours. This experiment was repeated three times with DEP exposure and three times without DEP exposure to determine effect of DEP exposure and reproducibility. Figure 7 shows that DEP exposed cells differentiated into myotubes with a high degree of orientation parallel of the electrodes while the unexposed cells differentiated only into randomly oriented myotubes. In these images, taken with an inverted microscope, looking up through the cells, the ITO array is not visible, but is oriented left to right, similar to Figure 6. Cell staining with Typan Blue showed that the aligned myotubes were still viable.

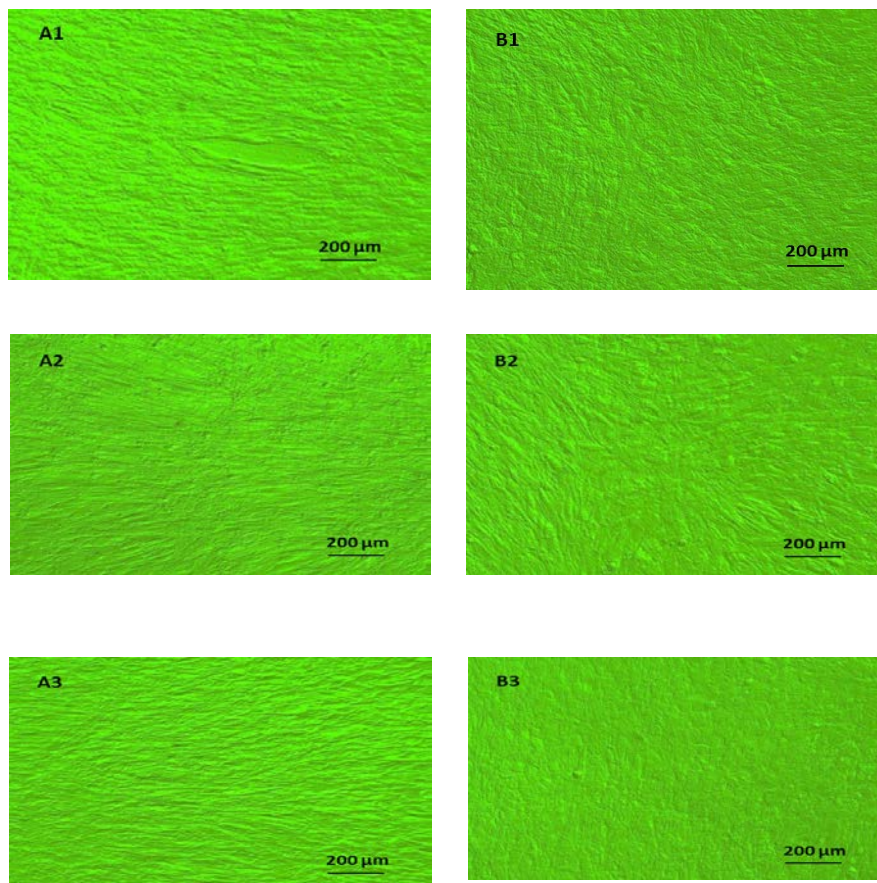


Figure 7: Images of differentiated C2C12 cells. A1, A2 and A3 were all exposed to intermittent DEP force and show horizontal orientation parallel to the electrode array. B1, B2, and B3 were not exposed to DEP force and show random orientation.

3. Conclusions

The array of interdigitated microelectrodes can orient differentiation of confluent C2C12 myoblast cells into myotubes parallel to the electrodes. This contactless alignment has advantages over the contact orientation because it avoids interactions with the walls of orienting channels. The larger sections of aligned tissues may be grown by scaling up the size of the array through extending the number and length of the electrodes. Our results provide guidelines to maximize the orienting force while applying a minimal electric field to avoid damage to biological cells: (1) the plateau in $\frac{dE}{dx}$ above an electrode-to-gap ratio of 1.0 suggests that array should have equally sized electrodes and gaps between them, (2) the rapid drop off of $\frac{dE}{dx}$ with increasing array height and a null gradient at 2 times of the electrode width suggests that the array should be placed as close as possible to the substrate, (3) the maximum value for $\frac{dE}{dx}$ when electrode widths are close to the array's height suggests that these parameters should be close to each other.

4. Recommendations

The limitations of this study have not fully investigated the long term effects of a DEP field on cell growth and viability. While attempts were made to limit the exposure the electric field while obtaining sufficient orientation, this process has not been optimized. The minimum intermittent exposure is currently unknown. Next steps would be to optimize the exposure for optimal cell viability after full tissue growth has been achieved. Further studies will also attempt to expand the size and height of the array to obtain aligned tissues suitable for grafting.

References

- [1]. Li, M., et al., A review of microfabrication techniques and dielectrophoretic microdevices for particle manipulation and separation. *Journal of Physics D-Applied Physics*, 2014. 47(6): p. 063001 1-29.
- [2]. Green, N.G., A. Ramos, and H. Morgan, Numerical solution of the dielectrophoretic and travelling wave forces for interdigitated electrode arrays using the finite element method. *Journal of Electrostatics*, 2002. 56(2): p. 235-254.
- [3]. Gunda, N.S.K. and S.K. Mitra, Dielectrophoresis for Manipulation of Bioparticles. 2011: p. 335-354.
- [4]. Holmes, D. and H. Morgan, Cell positioning and sorting using dielectrophoresis. *European Cells and Materials*, 2002. 4(Supple): p. 120-122.
- [5]. Jaramillo, M.d.C., et al., On-line separation of bacterial cells by carbon-electrode dielectrophoresis. *Electrophoresis*, 2010. 31(17): p. 2921-2928.
- [6]. Javanmard, M., et al., Use of negative dielectrophoresis for selective elution of protein-bound particles. *Analytical chemistry*, 2012. 84(3): p. 1432-1438.
- [7]. Lagally, E.T., S.-H. Lee, and H. Soh, Integrated microsystem for dielectrophoretic cell concentration and genetic detection. *Lab on a Chip*, 2005. 5(10): p. 1053-1058.
- [8]. Díaz, R. and S. Payen, Biological cell separation using dielectrophoresis in a microfluidic device. *Bio and Thermal Engineering Laboratory–University of California B (ed). <http://robotics.eecs.berkeley>*.

edu/%7Epister/245/project/DiazPayen.pdf, 2008.

- [9]. Arnold, W.M., Dielectrophoretic Cell Separation: Some Hints and Kinks. Proc. ESA Annual Meeting on Electrostatics, 2010: p. 1-11.
- [10]. Gascoyne, P.R. and J. Vykoukal, Particle separation by dielectrophoresis. *Electrophoresis*, 2002. 23(13): p. 1973.
- [11]. Markx, G.H., M.S. Talary, and R. Pethig, Separation of viable and non-viable yeast using dielectrophoresis. *Journal of biotechnology*, 1994. 32(1): p. 29-37.
- [12]. Adams, T., K. Leonard, and A. Minerick, Frequency sweep rate dependence on the dielectrophoretic response of polystyrene beads and red blood cells. *Biomicrofluidics*, 2013. 7(6): p. 064114.
- [13]. Jones, P.V., S.J. Staton, and M.A. Hayes, Blood cell capture in a sawtooth dielectrophoretic microchannel. *Analytical and bioanalytical chemistry*, 2011. 401(7): p. 2103-2111.
- [14]. Gagnon, Z. and H.C. Chang, Aligning fast alternating current electroosmotic flow fields and characteristic frequencies with dielectrophoretic traps to achieve rapid bacteria detection. *Electrophoresis*, 2005. 26(19): p. 3725-3737.
- [15]. Cheng, I.-F., et al., A continuous high-throughput bioparticle sorter based on 3D traveling-wave dielectrophoresis. *Lab on a Chip*, 2009. 9(22): p. 3193-3201.
- [16]. Dash, S. and S. Mohanty, Dielectrophoretic separation of micron and submicron particles: a review. *Electrophoresis*, 2014. 35(18): p. 2656-72.
- [17]. Muratore, M., et al., Biomarker-free dielectrophoretic sorting of differentiating myoblast multipotent progenitor cells and their membrane analysis by Raman spectroscopy. *Biomicrofluidics*, 2012. 6(3): p. 034113.
- [18]. LiáJeon, N., Dielectrophoresis switching with vertical sidewall electrodes for microfluidic flow cytometry. *Lab on a Chip*, 2007. 7(9): p. 1114-1120.
- [19]. Lewpiriyawong, N., C. Yang, and Y.C. Lam, Dielectrophoretic manipulation of particles in a modified microfluidic H filter with multi-insulating blocks. *Biomicrofluidics*, 2008. 2(3): p. 034105.
- [20]. Yu, C., et al., A three-dimensional dielectrophoretic particle focusing channel for microcytometry applications. *Microelectromechanical Systems, Journal of*, 2005. 14(3): p. 480-487.
- [21]. Norman, J.J. and T.A. Desai, Control of cellular organization in three dimensions using a microfabricated polydimethylsiloxane-collagen composite tissue scaffold. *Tissue engineering*, 2005. 11(3-4): p. 378-386.
- [22]. Deutsch, J., et al., Fabrication of microtextured membranes for cardiac myocyte attachment and orientation. *Journal of biomedical materials research*, 2000. 53(3): p. 267-275.
- [23]. Griscom, L., et al., Techniques for patterning and guidance of primary culture neurons on micro-electrode arrays. *Sensors and Actuators B: Chemical*, 2002. 83(1): p. 15-21.
- [24]. Dalby, M.J., et al., Increasing fibroblast response to materials using nanotopography: morphological and genetic measurements of cell response to 13-nm-high polymer demixed islands. *Experimental cell research*, 2002. 276(1): p. 1-9.
- [25]. Ainslie, K.M. and T.A. Desai, Microfabricated implants for applications in therapeutic delivery, tissue engineering, and biosensing. *Lab on a Chip*, 2008. 8(11): p. 1864-1878.
- [26]. Dalby, M.J., et al., Nucleus alignment and cell signaling in fibroblasts: response to a micro-grooved

- topography. *Experimental cell research*, 2003. 284(2): p. 272-280.
- [27]. Walboomers, X., et al., Growth behavior of fibroblasts on microgrooved polystyrene. *Biomaterials*, 1998. 19(20): p. 1861-1868.
- [28]. van Kooten, T.G., J.F. Whitesides, and A.F. von Recum, Influence of silicone (PDMS) surface texture on human skin fibroblast proliferation as determined by cell cycle analysis. *Journal of biomedical materials research*, 1998. 43(1): p. 1-14.
- [29]. Thakar, R.G., et al., Regulation of vascular smooth muscle cells by micropatterning. *Biochemical and biophysical research communications*, 2003. 307(4): p. 883-890.
- [30]. Suzuki, M., et al., Negative dielectrophoretic patterning with different cell types. *Biosensors and bioelectronics*, 2008. 24(4): p. 1043-1047.
- [31]. Burgarella, S., M. Bianchessi, and M. De Fazio, Numerical Modeling of Dielectrophoretic Forces Acting upon Biological Cells in Silicon Lab-On-Chip Devices. *COMSOL Users Conference*, 2007. 2007: p. 1-6.
- [32]. Matsue, T., N. Matsumoto, and I. Uchida, Rapid micropatterning of living cells by repulsive dielectrophoretic force. *Electrochimica Acta*, 1997. 42(20-22): p. 3251-3256.
- [33]. Suehiro, J. and R. Pethig, The dielectrophoretic movement and positioning of a biological cell using a three-dimensional grid electrode system. *Journal of Physics D-Applied Physics*, 1998. 31(22): p. 3298-3305.
- [34]. Chu, H.K., et al., Three-dimensional cell manipulation and patterning using dielectrophoresis via a multi-layer scaffold structure. *Lab on a Chip*, 2015. 15(3): p. 920-930.
- [35]. Hsiung, L.-C., et al., A planar interdigitated ring electrode array via dielectrophoresis for uniform patterning of cells. *Biosensors and Bioelectronics*, 2008. 24(4): p. 869-875.
- [36]. Ramón-Azcón, J., et al., Gelatin methacrylate as a promising hydrogel for 3D microscale organization and proliferation of dielectrophoretically patterned cells. *Lab on a Chip*, 2012. 12(16): p. 2959-2969.
- [37]. Albrecht, D.R., et al., Multiphase electropatterning of cells and biomaterials. *Lab on a Chip*, 2007. 7(6): p. 702-709.
- [38]. Pohl, H.A. and H. Pohl, *Dielectrophoresis: the behavior of neutral matter in nonuniform electric fields*. Vol. 80. 1978: Cambridge university press Cambridge.
- [39]. Lin, Y., Numerical modeling of dielectrophoresis. *Technical Reports from Royal Institute of Technology*, 2006: p. 1-44.